Published as: *Nature*. 2009 February 26; 457(7233): 1142–1145.

The subcellular organization of neocortical excitatory connections

Leopoldo Petreanu, **Tianyi Mao**, **Scott Sternson**, and **Karel Svoboda**
Janelia Farm Research Campus, Howard Hughes Medical Institute, Ashburn VA 20147, USA

Abstract

Understanding cortical circuits will require mapping the connections between specific populations of neurons 1, as well as determining the dendritic locations where the synapses occur 2. The dendrites of individual cortical neurons overlap with numerous types of local and long-range excitatory axons, but axodendritic overlap is not always a good predictor of actual connection strength 3-5. Here we developed an efficient Channelrhodopsin-2 (ChR2)-assisted method 6-8 to map the spatial distribution of synaptic inputs, defined by presynaptic ChR2 expression, within the dendritic arbors of recorded neurons. We expressed ChR2 in two thalamic nuclei, the whisker motor cortex and local excitatory neurons and mapped their synapses with pyramidal neurons in layers (L) 3, 5A, and 5B in the mouse barrel cortex. Within the dendritic arbors of L3 cells, individual inputs impinged onto distinct single domains. These domains were arrayed in an orderly, monotonic pattern along the apical axis: axons from more central origins targeted progressively higher regions of the apical dendrites. In L5 arbors different inputs targeted separate basal and apical domains. Input to L3 and L5 dendrites in L1 was related to whisker movement and position, suggesting a role of these signals in controlling the gain of their target neurons 9. Our experiments reveal exquisite specificity in the subcellular organization of excitatory circuits.

We recorded from pyramidal neurons in neocortical brain slices containing ChR2-expressing axons 7(Fig. 1a). To map the dendritic locations of input from ChR2-positive axons (Fig. S1) we used a laser to depolarize these axons only in the vicinity of the laser beam (i.e. with action potentials blocked), triggering local glutamate release (subcellular Channelrhodopsin-2 Assisted Circuit Mapping, sCRACM). We blocked Na^+ channels (1 μM tetrodotoxin,TTX) and the K^+ channels that are critical for repolarization of the axon (200 nM α-dendrotoxin or 100 μM 4-aminopyridine, 4-AP) (Fig. 1 b)10. Under these conditions, photostimulation with short (1 ms) light pulses (< 2 mW) triggered robust excitatory postsynaptic currents ($EPSC_{sCRACM}$) (Fig. 1 b). Higher light intensities caused larger $EPSC_{sCRACM}$ amplitudes (Fig. 1 c) and shorter onsets (Fig. S2). As the cylindrical laser beam was scanned over the dendrites of a recorded neuron (map pattern: 12 × 24 grid; 50 μm spacing), $EPSC_{sCRACM}$ were detected only when the laser beam overlapped with the dendritic arbor of the recorded cell and with ChR2-positive axons (Fig. 1 b, d-f), indicating

Author contributions
LP and KS conceived and designed the experiments. LP performed the experiments with help from TM (viral injections in M1 and related recordings). SS provided critical reagents. LP and KS analyzed the data and wrote the paper.

Supplementary Information is linked to the online version of the paper at www.nature.com/nature.

Methods Summary
Specific neuronal populations were labeled with ChR2 *in vivo* either by *in utero* electroporation 7, 28(L2/3 pyramidal cells), Adeno-Associated Virus (AAV) infection (VPM, POm, M1), or infection with a Cre recombinase-dependent AAV virus 29 in mice expressing Cre (L4) 30. Acute coronal slices were from young adult (P26-34) mice. Pyramidal neurons in L3 and L5 were recorded in voltage clamp at room temperature (22-24°C). Photostimulation was with blue (wavelength, 473nm) laser pulses (duration, 1ms; inter-stimulus interval, 400 ms; beam diameter 6-16 μm) in the presence of TTX (1 μM), 3-((R)-2-Carboxypiperazin-4-yl)-propyl-1-phosphonic acid (CPP ,5 μM), and 4-AP (100 μM).

that under these conditions light depolarizes ChR2-positive axons to cause local release of neurotransmitter. Converting $EPSC_{sCRACM}$ into pixel values ($EPSC_{sCRACM}$ averaged over a time window 0 – 75 ms post-stimulus) provides a two-dimensional 'image' of the distribution of specific input within the dendritic arbors of the recorded cell (Fig. 1 e,f). Measurements of the point-spread-function revealed that sCRACM maps specific types of input with ~ 60 μm spatial resolution (Fig. S3).

$EPSC_{sCRACM}$ amplitudes depend on the density of ChR2-positive axons, the fraction of axons that make synapses with the recorded neuron, the strength of the synapses, and their electrotonic distance from the soma 11 (see Methods). Since the density of ChR2-positive axons varies between preparations, sCRACM maps were normalized to the largest pixels within a map and thus represent the relative strength of input within the dendritic tree. Repeated sCRACM maps where reproducible at the level of single pixels (Fig. S4), and the structure of peak-normalized maps was similar across a large range of light intensities (Fig. S4).

Multiple types of axon overlap with the dendrites of cortical neurons 5, 12-17. Some axons arise locally 5, 14, 18, whereas others ascend from the thalamus 15, 16 or descend from higher cortical areas 17. Which axons in a target region connect with a particular cell type? And what are the spatial distributions of input within the dendritic tree? To answer these questions we expressed ChR2 in five distinct axonal populations (in separate experiments) that overlap with pyramidal cell dendrites in the barrel cortex (Fig. S5). The spatial distribution of labeled axons in the barrel cortex was largely in agreement with previous anatomical studies (Fig. S5). Projections from the ventral posterior medial nucleus (VPM) of the thalamus were focused in L4 and at the border of L5 and L6 (Fig. 2 a and Fig. S5) 16, but diffuse axons were found throughout all cortical layers 15. L4 axons arborized in L4 and ascended into L2/3, up to the lower edge of L1 18; a weaker projection descended into L5 and L6 18. Axons from L2/3 pyramidal cells arborized within L2/3 and on the border of L5A and L5B 7, 14. Axons from the primary whisker motor cortex (M1) arborized densely in L1, and more diffusely in L5 and L6 17. A dense bundle of ascending M1 axons was often apparent next to the most medial barrels (Fig. 2 a, arrow head). Axons from the posterior medial nucleus (POm) of the thalamus were focused in L5A, and more weakly in L1 15.

We mapped specific types of input within the dendritic trees of individual L3 cells (Fig. 2a). Maps were then averaged across cells either aligned on the pia (Fig.2 b), to visualize the laminar location of the inputs, or aligned on the soma, to measure the location of the inputs relative to the soma (Fig.2 c). L3 cells received input from all five projections. Each input overlapped with a single contiguous dendritic subregion. Ascending VPM→L3 input was focused on the bottom part of the basal dendritic arbors. Input from ascending L4→L3 axons was centered on the soma and basal arbor, above the input from VPM. Input from recurrent L2/3→L3 axons was mostly in the upper basal dendrites and the apical oblique dendrites, above the input from L4 (see also Fig.S6). Feedback from M1 targeted the tuft branches in L1, above the input from L2/3. The positions of VPM, L4, L2/3, and M1 input along the apical axis of L3 neurons mirrors the flow of excitation within the cortical circuit: more peripheral (central) input impinges on lower (higher) parts of the dendritic arbor. During somatosensation L3 neurons thus receive an ascending wave of excitatory input. POm→L3 input was weighted towards L1, although it was distributed relatively broadly, spanning most of the dendritic arbor.

We next mapped the same group of five inputs within the dendrites of L5 pyramidal neurons. Both L5A and L5B pyramidal cells received input from L4, L2/3, M1 and VPM (Fig.3 a,b and S7) . To quantify the strength of input from defined axonal projections across

postsynaptic cells in different layers, we recorded from pairs of cells in the same column with identical laser powers (Supplemental table 1). L5B cells received 62-fold less input from POm compared to L5A cells, despite pronounced overlap between L5B dendrites and POm axons (Fig. 3c,d, Fig. S7 and Supplemental table 1) (dendritic length: L5A pyramids (n=12), in L1, 871±546 μm , in L5A, 2158±899 μm; L5B pyramids (n=13), in L1, 1609 ±732 μm, in L5A, 761 ± 350 μm). L5A, but not L5B, pyramidal cells received significant input from POm. This confirms that average cortical connectivity between populations of neurons cannot always be deduced from the structure of axons and dendrites alone 3, 4, 5 . Because L5B pyramidal neurons constitute the main projection from barrel cortex to POm 19, there appears to be no disynaptic loop between these two areas.

In contrast to L3 cells, the inputs on L5 cells were not limited to a single compartment, but were split into basal and apical domains (Fig.3 and Fig. S7), reinforcing the view that large pyramidal neurons consist of multiple, weakly coupled compartments 20. Here we describe the inputs to L5B neurons (Fig. 3), and then highlight the differences with L5A neurons (Fig. S7). VPM→L5B input was distributed along most of the dendritic arbor, but was most prominent on the basal dendrites and in L4. L4→L5B input was centered on the basal dendrites, overlapping with VPM input; weak input was also detected along the apical dendrite up to the edge of L1. L2/3→L5B input was focused on the upper basal and apical oblique dendrites, as well as on the apical tuft in L2. M1→L5B input was on the basal dendrites and on the apical tuft in L1.

Inputs to L5A pyramidal neurons similarly targeted dual dendritic compartments (Fig. S7), with some differences. POm →L5A input was prominent, both on the basal dendrites and the apical tuft in L1. Unlike for L2/3→L5B input, L2/3→L5A input was centered on the basal dendrites (Fig. 4 a and Fig. S7). For all L5 neurons taken together, there was a monotonic relationship between the laminar position of the recorded cell and the location of L2/3 input relative to the soma position (Fig. 4 b-d). The axodendritic overlap of L2/3 axons and L5 dendrites is likely an important factor determining the subcellular location of L2/3→L5 input.

sCRACM maps functional neural circuits with subcellular resolution. Since sCRACM maps are based on somatic measurements of synaptic currents generated in the dendrites signal attenuation due to dendritic filtering influences the structure of the maps. For example, input on the apical tufts of L5 neurons could be reduced several-fold compared to more proximal input 11. sCRACM maps thus represent a “somatocentric” view of the dendritic distribution of synaptic input, where electrotonically distant synapses will appear relatively weak (Figure S8).

We mapped input from VPM, L4, L2/3, M1 and POm, within the dendritic arbors of L3 and L5 neocortical pyramidal cells. L3 and L5 cells received input from most axonal populations, with the exception of POm→L5B. Some connections (VPM→L3, VPM→L5A, VPM→L5B, POm→L5A, L4→L3, L4→L5A, L2/3→L3, L2/3→L5A, L2/3→L5B) have been previously characterized 3, 14, 18, 21, 22, whereas others (M1→L3, M1→L5A, M1→L5B, POm→L3, L4→L5B,) were previously unknown.

We identified several connections in L1: M1→L3, M1→L5A, M1→L5B, POm→L3 and POm→L5A. Axons from VPM, L2/3 and L4 did not contribute significantly to L1 input. POm neurons are thought to encode aspects of whisker position 23 and whisker M1 carries signals related to voluntary whisker control 24. Our findings suggest that synapses in L1 carry signals related to whisker movement and position.

The spatial segregation of specific types of input within dendritic arbors might subserve several functions. Segregated inputs are less likely to interact at the level of synaptic

plasticity 25. Spatially clustered coactive synapses are more efficacious in driving postsynaptic neurons than spatially distributed synapses 26, 27. For a fixed number of synapses, spatial segregation of different axonal populations within dendritic arbors might thus serve to strengthen the effective coupling between pre- and postsynaptic populations.

Supplementary Material

Refer to Web version on PubMed Central for supplementary material.

Acknowledgments

We thank A. Karpova for help with viral constructs, G. Oliver and B. Xu for the Six3Cre mouse line, D. Chklovskii, G. Shepherd, and Q. Wen for comments on the manuscript, Y. Yu for the model of the K_d channel, and T. O'Connor for software development.

Methods

Electrophysiology and photostimulation

Neurons were patched with borosilicate pipettes (resistance 4–6 MΩ). The intracellular solution contained in mM (in mM) 128 Kgluconate, 4 $MgCl_2$, 10 HEPES, 1EGTA, 4 Na_2ATP, 0.4 Na_2GTP, 10 sodium phosphocreatine, 3 sodium L-ascorbate and 0.015 Alexa-594 (Molecular Probes) (pH 7.25; 290 mOsm). Cells were recorded at depths of 50 to 95 μm in the brain slice. Data were acquired using custom programs (Ephus, available at https://openwiki.janelia.org/). Photostimulation was with a blue laser (473 nm; Crystal Laser). The beam's position was controlled with galvanometers (Cambridge Scanning, Inc.). The beam was delivered through an air immersion objective (4×; 0.16 NA; UPlanApo, Olympus). The optics were designed to generate a nearly cylindrical beam (~6-16 μm, full-width at half max at the focal plane). The duration and intensity of the light pulses were controlled with a Pockels cell (ConOptics) and a shutter (Uniblitz).

For sCRACM mapping we delivered light pulses (duration, 1ms; inter-stimulus interval, 400 ms) on a 12 × 24 grid with 50 μm spacing (Fig. 1 d). The grid area (0.6 × 1.2 mm^2) included the entire thickness of the cortical grey matter. Stimuli were given in a spatial sequence pattern designed to maximize the time between stimuli to neighboring spots 31. To avoid sequence-specific responses during consecutive mapping we flipped and rotated the stimulus pattern between maps. TTX (1 μM), CPP (5 μM), and 4-AP (100 μM) were added to the bath. Without 4-AP (or α-dendrotoxin, Alomone Labs, Israel, 200 nM), TTX (1 μM) abolished 98 ± 1.9 % of the EPSCs evoked in the absence of drugs (6 cells, 573 sites), even at high light intensities (> 1 mW) (Fig. 1b). When mapping inputs from L4 axons we also added Bicuculline (10 μM) to block contributions from GABAergic neurons in L4 30. $EPSC_{sCRACM}$ were recorded in voltage clamp (−75 mV). Access resistances were < 40 MOhm and stable (< 20% change during the experiment); resting potentials were less than −55 mV.

$EPSC_{sCRACM}$ have relatively long delays (mean, 10.4 ± 2.5 ms; L2/3→L5A perisomatic responses; < 110 μm from the soma; 146 sites; 18 cells) (Fig. S2), likely reflecting the slow charging and discharging of the axonal membrane (Fig. S9). The delays varied across photostimulation sites (range: 6.4 - 21 ms) and $EPSC_{sCRACM}$ rise- (mean (10 – 90 %): 6.5 ± 3.1 ms; range: 2.4 - 18.3 ms) and decay-times (mean: 35 ± 28 ms; range: 6.2 - 160 ms) were long. $EPSC_{sCRACM}$ on occasion displayed multiple peaks. Minimal stimulation experiments (Fig. S2c) revealed that unitary currents were slightly desynchronized at a single photostimulation location (latency jitter, 1.03±0.5 ms, n = 6) and highly desynchronized across different locations (latency range, 10.4-17.2 ms, mean 15.2±3 ms , n=6) (Fig. S2).

The temporal smearing of the $EPSC_{sCRACM}$ waveform is therefore dominated by differences in latencies across different synapses. The risetime of the responses increased with distance to the soma, both along the apical and basal dendrites, consistent with filtering expected from cable theory (Fig. S2) 32, 33.

For each recorded cell, laser powers were adjusted to cause $EPSC_{sCRACM}$ with peak amplitudes of approximately - 75 pA (L2/3 pyramidal neurons, −72±47 pA; L5 pyramidal neurons: −84±45 pA). The corresponding laser powers varied over one order of magnitude (120 μW-1.9 mW at the specimen plane), reflecting variations in the fraction of ChR2-positive axons and ChR2 expression levels across mice. sCRACM maps were repeated 2-5 times for each cell (Figure S4). After the recordings dendritic arbors were imaged using fluorescence microscopy (Qimaging, Surrey, Canada) and subsequently processed for biocytin staining and reconstructed. Only data from neurons where the apical dendrites ran parallel to the slice surface were included in the analysis.

Since photostimulation was with a cylindrical beam, sCRACM maps represent the 2-D projections of the 3-D distribution of inputs. As a consequence, the peak values of the distribution of inputs were sometimes centered on the somata, although somata are mostly devoid of excitatory synapses (Fig. 2 and Fig. 3). This is analogous to the 2-D projection of the density of basal dendrites, which also peaks on the soma (Fig. 2, 3 and S7). Furthermore, under our conditions the sCRACM resolution was ~ 60 μm, large compared to the diameters of most somata.

Data Analysis

Individual pixels of sCRACM maps at position x, y ($Q(x, y)$) were computed as the mean $EPSC_{sCRACM}$ amplitude in a response window from 0 to 75 ms after the stimulus, and thus are a measure of charge. For consistency with previous studies, and because synaptic current is a more familiar unit, data are given in units of picoamperes (pA). Q is given by

$$1/g\,(r) = 1 - 2^{(-r/\lambda)},$$

ρ_a and ρ_b are the density of axons and dendrites respectively. f is the filling fraction, defined as the fraction of axons making synapses with nearby dendrites 34. q is the charge per synapse per light flash. $g(L)$ is the dendritic attenuation as a function of electrotonic distance, $L(x,y)$, between the site of photostimulation and the soma. Because of dendritic attenuation, Q provides a somatocentric view of the synaptic input (see Supplementary Discussion). Since ρ_a, and possibly q, depend on details of the gene transfer method, it is challenging to compare the strengths of different projections onto the same cell. Since ρ_a varies between preparations, sCRACM maps were normalized to the largest pixels within a map and thus represent the relative strength of input within the dendritic tree.

Averaged $EPSC_{sCRACM}$ were scored as non-zero if their amplitudes (0-50 ms poststimulus) were larger than 5x the standard deviation of the baseline (Fig. 1 e, 2a, 3 a, 4 a, S3 and S7). Maps were either aligned on the soma or on the pia. In the case of alignment to the pia it was necessary to correct for variations in cortical thickness; individual maps were therefore morphed by linear interpolation to a template based on the average cortical thickness. Similarly, the cortical depth of individual neurons (Fig. 4) was also normalized to the average depth across slices. Individual maps are presented as raw pixel images, whereas group averages are linearly interpolated without smoothing (for display only). To measure the density of L2/3 axons (Fig. 4 b) we measured and peak normalized mCherry

fluorescence along the cortical axis in L4 through L6 in *in utero* electroporated animals (n=5).

sCRACM Resolution

The effective resolution of sCRACM mapping can be inferred from the point-spread-function. We measured the point-spread-function from the spatial distribution of the photostimulation sites that produce detectable responses in the vicinity of isolated dendritic branches. L5A cells often received input from L2/3 neurons along a single unbranched apical dendrite within L2/3 (Fig. S3). To measure sCRACM resolution, we first identified the peak of L2/3 input on the apical dendrites of L5A cells within L2/3. We next photostimulated in a line across the apical dendrite, through the peak of L2/3 input (12 positions, 15 μm spacing between stimuli, inter-stimulus interval, 6 s) (Fig. S3 a). Since the activated synapses were on a single dendritic branch in the vicinity of the photostimuli, the spatial distribution of responses represents a measure of the spatial resolution. After the experiment the dendritic arbor of the recorded neurons were reconstructed. Only cells where the apical dendrite did not ramify within 100 μm the photostimulation sites were included for analysis. For the light intensities used for sCRACM mapping, the full-width-at-half-max (FWHM) of the spatial profile of the responses was 59 ± 14 μm (n = 4) (Fig. S3 b-c). Higher laser intensities degraded the resolution slightly.

To verify this resolution estimate within our data set, we identified stretches of unbranched L5 apical dendrites that received input from ChR2-positive axons originating either in VPM, L4, or L2/3. Only inputs separated by at least 100 μm from branchpoints were used. In addition, to avoid over-representation of a subset of inputs, we only scored inputs that were at least 100 μm apart. Detectable $EPSC_{sCRACM}$ were only evoked within 75 μm of the apical dendrite (Fig. S3 d,e). We conclude that sCRACM maps specific types of input with ~ 60 μm spatial resolution.

Data in the text are given as mean ± SD.

References

31. Shepherd GM, Pologruto TA, Svoboda K. Circuit analysis of experience-dependent plasticity in the developing rat barrel cortex. Neuron. 2003; 38:277–89. [PubMed: 12718861]
32. Williams SR, Stuart GJ. Site independence of EPSP time course is mediated by dendritic I(h) in neocortical pyramidal neurons. J Neurophysiol. 2000; 83:3177–82. [PubMed: 10805715]
33. Nevian T, Larkum ME, Polsky A, Schiller J. Properties of basal dendrites of layer 5 pyramidal neurons: a direct patch-clamp recording study. Nat Neurosci. 2007; 10:206–14. [PubMed: 17206140]
34. Stepanyants A, Hof PR, Chklovskii DB. Geometry and structural plasticity of synaptic connectivity. Neuron. 2002; 34:275–88. [PubMed: 11970869]

References

1. Douglas RJ, Martin KA. Mapping the matrix: the ways of neocortex. Neuron. 2007; 56:226–38. [PubMed: 17964242]
2. London M, Hausser M. Dendritic computation. Annu Rev Neurosci. 2005; 28:503–32. [PubMed: 16033324]
3. White EL. Specificity of cortical synaptic connectivity: emphasis on perspectives gained from quantitative electron microscopy. J Neurocytol. 2002; 31:195–202. [PubMed: 12815239]
4. Dantzker JL, Callaway EM. Laminar sources of synaptic input to cortical inhibitory interneurons and pyramidal neurons. Nat Neurosci. 2000; 3:701–7. [PubMed: 10862703]

5. Shepherd GMG, Stepanyants A, Bureau I, Chklovskii DB, Svoboda K. Geometric and functional organization of cortical circuits. Nature Neuroscience. 2005; 8:782–790.
6. Nagel G, et al. Channelrhodopsin-2, a directly light-gated cation-selective membrane channel. Proc Natl Acad Sci U S A. 2003; 100:13940–5. [PubMed: 14615590]
7. Petreanu L, Huber D, Sobczyk A, Svoboda K. Channelrhodopsin-2-assisted circuit mapping of long-range callosal projections. Nat Neurosci. 2007; 10:663–8. [PubMed: 17435752]
8. Zhang F, Wang LP, Boyden ES, Deisseroth K. Channelrhodopsin-2 and optical control of excitable cells. Nat Methods. 2006; 3:785–92. [PubMed: 16990810]
9. Larkum ME, Senn W, Luscher HR. Top-down dendritic input increases the gain of layer 5 pyramidal neurons. Cereb Cortex. 2004; 14:1059–70. [PubMed: 15115747]
10. Shu Y, Yu Y, Yang J, McCormick DA. Selective control of cortical axonal spikes by a slowly inactivating K+ current. Proc Natl Acad Sci U S A. 2007; 104:11453–8. [PubMed: 17581873]
11. Williams SR, Mitchell SJ. Direct measurement of somatic voltage clamp errors in central neurons. Nat Neurosci. 2008; 11:790–8. [PubMed: 18552844]
12. Binzegger T, Douglas RJ, Martin KA. A quantitative map of the circuit of cat primary visual cortex. J Neurosci. 2004; 24:8441–53. [PubMed: 15456817]
13. Gilbert CD. Microcircuitry of the visual cortex. Ann. Rev. Neurosci. 1983; 6:217–247. [PubMed: 6132585]
14. Feldmeyer D, Lubke J, Sakmann B. Efficacy and connectivity of intracolumnar pairs of layer 2/3 pyramidal cells in the barrel cortex of juvenile rats. J Physiol. 2006; 575:583–602. [PubMed: 16793907]
15. Lu SM, Lin RCS. Thalamic afferents of the rat barrel cortex: a light- and electron-microscopic study using *Phaseolus vulgaris* leucoagglutinin as an anterograde tracer. Somatosens. Mot. Res. 1993; 10:1–16. [PubMed: 8484292]
16. Koralek KA, Jensen KF, Killackey HP. Evidence for two complementary patterns of thalamic input to the rat somatosensory cortex. Brain Res. 1988; 463:346–51. [PubMed: 2461788]
17. Veinante P, Deschenes M. Single-cell study of motor cortex projections to the barrel field in rats. J Comp Neurol. 2003; 464:98–103. [PubMed: 12866130]
18. Lubke J, Roth A, Feldmeyer D, Sakmann B. Morphometric analysis of the columnar innervation domain of neurons connecting layer 4 and layer 2/3 of juvenile rat barrel cortex. Cereb Cortex. 2003; 13:1051–1063. [PubMed: 12967922]
19. Hoogland PV, Welker E, Van der Loos H. Organization of the projections from barrel cortex to thalamus in mice studied with Phaseolus vulgaris-leucoagglutinin and HRP. Exp Brain Res. 1987; 68:73–87. [PubMed: 2826209]
20. Mainen ZF, Sejnowski TJ. Influence of dendritic structure on firing pattern in model neocortical neurons. Nature. 1996; 382:363–366. [PubMed: 8684467]
21. Bureau I, von Saint Paul F, Svoboda K. Interdigitated Paralemniscal and Lemniscal Pathways in the Mouse Barrel Cortex. PLoS Biol. 2006; 4:e382. [PubMed: 17121453]
22. Thomson AM, Bannister AP. Interlaminar connections in the neocortex. Cereb Cortex. 2003; 13:5–14. [PubMed: 12466210]
23. Yu C, Derdikman D, Haidarliu S, Ahissar E. Parallel Thalamic Pathways for Whisking and Touch Signals in the Rat. PLoS Biol. 2006; 4:e124. [PubMed: 16605304]
24. Berg RW, Kleinfeld D. Vibrissa movement elicited by rhythmic electrical microstimulation to motor cortex in the aroused rat mimics exploratory whisking. J Neurophysiol. 2003; 90:2950–63. [PubMed: 12904336]
25. Harvey CD, Svoboda K. Locally dynamic synaptic learning rules in pyramidal neuron dendrites. Nature. 2007; 450:1195–200. [PubMed: 18097401]
26. Polsky A, Mel BW, Schiller J. Computational subunits in thin dendrites of pyramidal cells. Nat Neurosci. 2004; 7:621–7. [PubMed: 15156147]
27. Losonczy A, Magee JC. Integrative Properties of Radial Oblique Dendrites in Hippocampal CA1 Pyramidal Neurons. Neuron. 2006; 50:291–307. [PubMed: 16630839]
28. Saito T, Nakatsuji N. Efficient gene transfer into the embryonic mouse brain using in vivo electroporation. Dev Biol. 2001; 240:237–46. [PubMed: 11784059]

29. Atasoy D, Aponte Y, Su HH, Sternson SM. A FLEX switch targets Channelrhodopsin-2 to multiple cell types for imaging and long-range circuit mapping. J Neurosci. 2008; 28:7025–30. [PubMed: 18614669]

30. Liao GY, Xu B. Cre Recombinase-mediated Gene Deletion in Layer 4 of Murine Sensory Cortical Areas. Genesis. 2008; 46:289–293. [PubMed: 18543315]

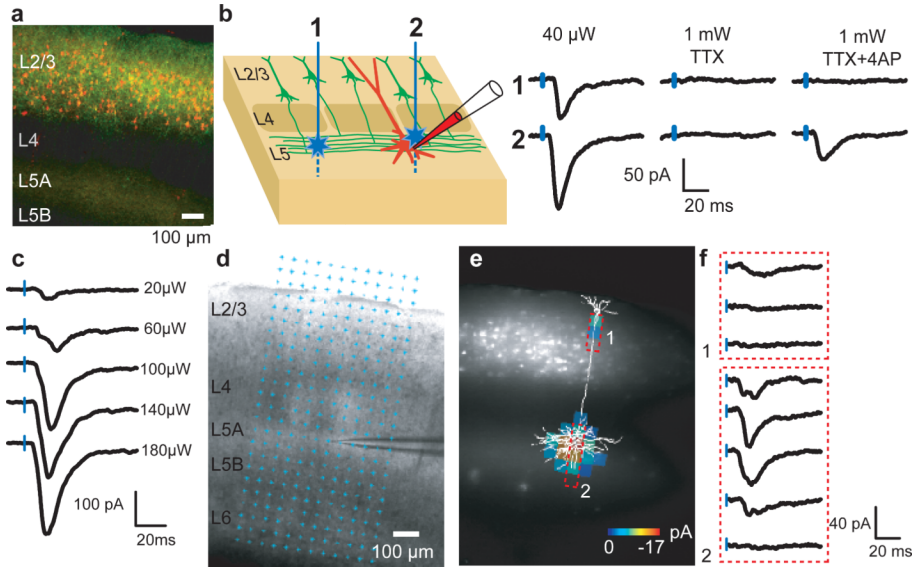

Figure 1. Subcellular Channelrhodopsin-2-Assisted Circuit Mapping (sCRACM)

a, Confocal image showing L2/3 neurons expressing mCherry (red) and ChR2-Venus (green) in the barrel cortex. **b,** Left, Schematic of the photostimulation geometry. Right, EPSCs evoked by photostimuli corresponding to the locations indicated in the schematic. Blue ticks indicate the laser pulse. Laser power is indicated on top. **c,** $EPSC_{sCRACM}$ evoked by photostimulation with increasing laser powers (right). **d,** Brightfield image of a brain slice showing the recording pipette and the photostimulation grid (blue dots). **e**, sCRACM map overlayed on a fluorescence image, showing ChR2-positive neurons, and the reconstructed dendrite of the recorded neuron (same experiment as d). Non-zero $EPSC_{sCRACM}$ are color-coded to represent mean amplitude. **f**, $EPSC_{sCRACM}$ recorded in the boxed regions in Panel e.

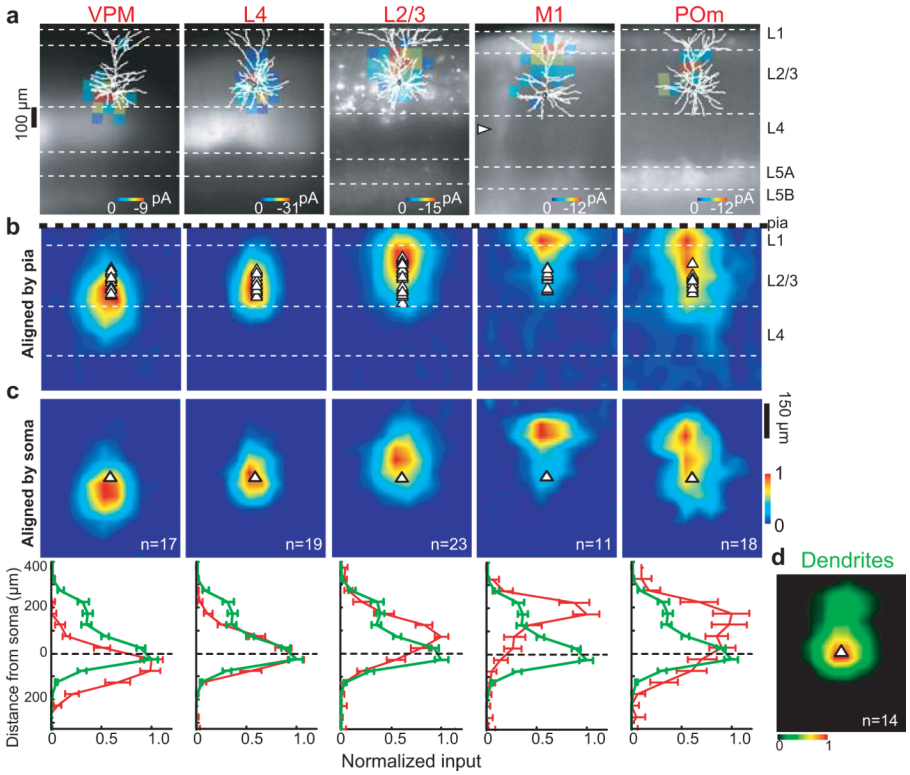

Figure 2. Subcellular distribution of inputs onto L3 pyramidal neurons

a, Examples of sCRACM maps overlaid on reconstructed dendrites and fluorescence images showing ChR2-positive axons (VPM, M1 and POm) or axons and dendrites (L2/3 and L4). White arrow head, bundle of ascending axons from M1. **b,** Group averages aligned by pia position (White triangles, soma position). **c**, top: Group averages aligned by soma position ; bottom: vertical profiles of the distribution of synaptic input (red) and the dendritic length density (green; from d). **d,** Average normalized dendritic length density of L3 pyramidal neurons. Error bars, s.e.m.

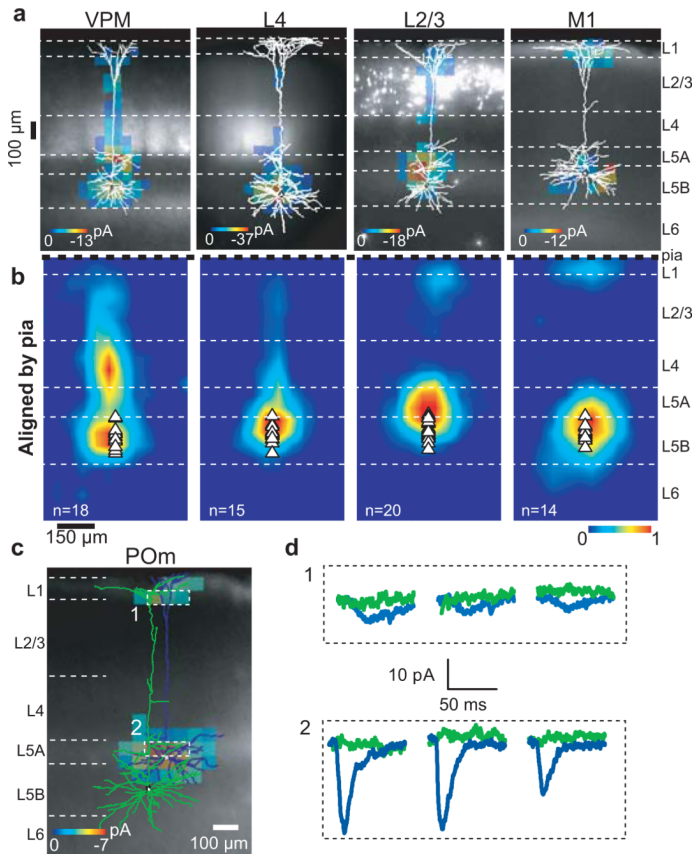

Figure 3. Subcellular distribution of inputs onto L5B pyramidal neurons

a, Examples of sCRACM maps overlaid on reconstructed dendritic arbors and fluorescence images. **b,** Group averages aligned by pia position. White triangles, soma position. **c,** sCRACM map of POm input onto a L5A pyramidal cell (blue). No responses were detected on the L5B neuron (green). **d**, $EPSC_{sCRACM}$ recorded on the L5A neuron (blue) or the L5B neuron (green) when photostimuating the boxed regions in Panel c . The stimulus occurred at the beginning of each trace.

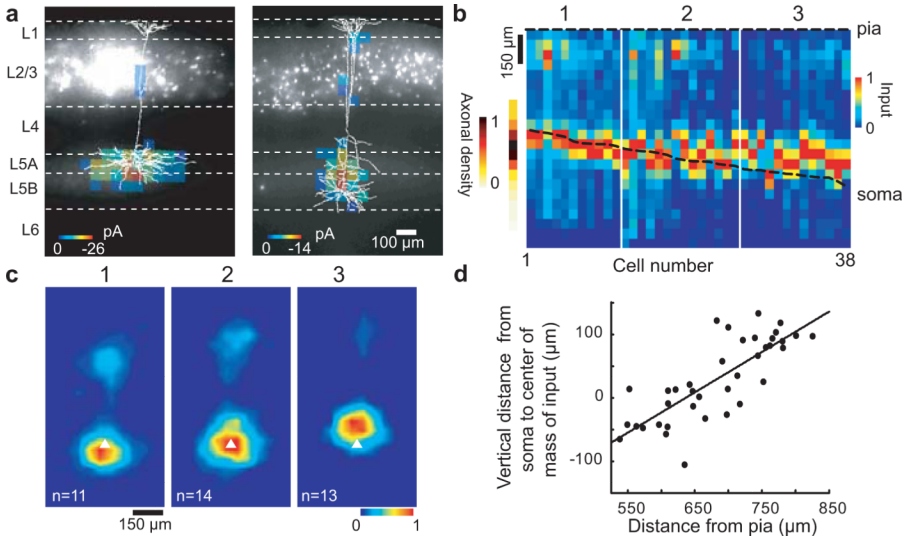

Figure 4. The laminar position of L5 pyramidal neurons determines the dendritic location of L2/3 inputs

a, Examples of the subcellular distribution of L2/3 input on superficial (L5A) (left) or deep (L5B) (right) pyramidal neurons. **b,** Vertical profiles of the subcellular distribution of L2/3→L5 inputs. Each column represents one cell, ordered by cortical depth. Cells were aligned by pia position. The relative density of L2/3 axons in the deep layers is indicated to the left of the panel. **c,** Average subcellular location of L2/3 input (aligned by soma position) of L5 cells grouped by increasing distance from the pia (groups correspond to the white lines in b).**d,** Plot of the vertical distance from the soma to the center of mass of L2/3 input on the perisomatic region (< 285 μm from the soma) of L5 pyramidal neurons vs. cortical depth. The line is a regression fit.